ARTICLE

Effect of halide solid solution on the structure, phase transition behaviour and dielectric properties of DabcoH$^+$ chains

Received 00th January 20xx,
Accepted 00th January 20xx

DOI: 10.1039/x0xx00000x

Yuki Ohishi,[a] Kohei Sambe,[b] Tomoyuki Akutagawa,[b,c] Atsuko Masuya-Suzuki,[a,d] and Ryo Tsunashima*[a,d]

The 1,4-diazabicyclo[2.2.2]octane (dabco) forms one-dimensional chains through intermolecular N-H$^+$···N hydrogen bonds and shows ferroelectricity originated from proton transfer. The size of polarized domain differs depending on the size, symmetry, and polarizability of the counter anions. Herein, two binary halide solid solutions of dabcoHCl with dabcoHBr (**ClBr**) and dabcoHBr and dabcoHI (**BrI**) were prepared and the temperature dependence of the structure of single crystal and phase transition behaviour were investigated. Solid solution of the **ClBr** contains 3% of Cl^- in dabcoHBr, and thus latice length as well as space group and volutme are almost same as those fo dabcHBr. Phase transition temperature from hydrogen boded structure to ion-paring structure decreased from 458 K to 440 K by mixing Cl^-. On the other hand, solid solution **BrI** was formed with all proportional solid solution and whose crystallographic parameters characterized by single crystal X-ray (XRD) diffraction analysis well obeyed to Vegard's law. Phase transition behavious were investigatged for single crystal of Br:I=8:2 (**Br$_{0.80}$I$_{0.20}$**) by temperature variable single crystal XRD analysis and we revealed that new structural regime appeared at 250-373 K in which intermolecular N-H$^+$···N hydrogen bond was weaken. It was also revealed that this is ferroelectric phase as well as original dabcoHBr. At high temperature range, phase transition from hydrogen bonded phase to ion-par phase was observed at 435 K, which is lower than 458 K of dabcoHBr.

Introductions

Ferroelectric materials possess various properties including piezoelectricity, pyroelectricity, and nonlinear optical properties. These characteristics enable these material applications in memory, capacitors, and thermal sensors.[1-3] However, these metal-containing ferroelectrics often include metals harmful to both the environment and human health, such as lead zirconate titanate (PZT) and barium titanate (BTO). These macroscopic ferroelectrics originated from a uniform arrangement of dipole moments. Conversely, there is another type of ferroelectrics known as relaxor ferroelectrics which is a system with inhomogeneous polarized domains. Relaxor ferroelectrics have a different mechanism of polarization inversion in contrast to common macroscopic ferroelectrics. Polarized domains are formed at mesoscopic scales and grow by an applied electric field.[4–8] They exhibit high dielectric and piezoelectric properties and broad temperature-frequency dispersion. These materials have been used in energy storage devices and piezoelectric actuators, for example. Metal-containing ferroelectrics are often relaxor ferroelectrics in the case of perovskite-type composite oxides with chemical formula $A(BB')O_3$. Relaxor ferroelectricity appears with strong covalent Pb ions in A, metal ions with low valence in B and d_0 transition metal ions with high valence in B'.[9–12] Thus, metal-containing relaxor ferroelectrics are being understood with design guidelines based on metal ion selectivity.

Conversely, metal-free ferroelectrics composed of organic molecules and/or halides have advantages in environmental and humane friendliness in addition to lightweight and easy processing.[13-18] The mechanism of ferroelectricity of the metal-free ferroelectrics differs from metal-containing ferroelectrics.

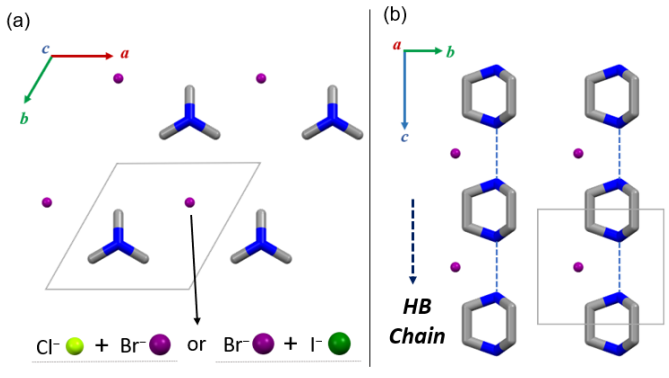

Fig. 1 Crystal structure of dabcoHX in (a) *ab* and (b) *bc* planes (C: grey, N: blue, Cl: light green, Br: purple, I: green). H atoms are omitted for clarity.

[a] *Graduate School of Sciences and Technology for Innovation, Yamaguchi University, Yoshida 1677-1, Yamaguchi, 753-8512, Japan.*
[b] *Graduate School of Engineering, Tohoku University, Sendai 980-8577, Japan.*
[c] *Institute of Multidisciplinary Research for Advanced Materials (IMRAM), Tohoku University, Sendai 980-8577, Japan*
[d] *Chemistry Course, Faculty of Science, Yamaguchi University, Yoshida 1677-1, Yamaguchi, Japan*

† Electronic Supplementary Information (ESI) available: [details of any supplementary information available should be included here]. See DOI: 10.1039/x0xx00000x

The mechanism of the metal-containing ferroelectrics is the displacement of atoms from centrosymmetric positions. In contrast, the metal-free ferroelectrics include orientational polarization of the molecules by inversing their orientation by the outer electric field and displacement of the proton in the hydrogen bond at the proper interatomic distances.

Several hydrogen-bonded ferroelectrics have been reported to exhibit spontaneous polarization comparable to those of metal-containing ferroelectrics at around room temperature.[19-24] One of these is dabcoHA (A = BF_4^-, ClO_4^-, ReO_4^-), dabco = 1,4-diazabicyclo[2.2.2]octane.[25-27] The structure is formed by dabcoH$^+$ forming one-dimensional hydrogen-bonded chains (Fig. 1). The counter anions A^- are distributed in the space of the dabcoH$^+$ chain and bridging them. The mechanism of ferroelectricity is proton transfer in hydrogen bonding, as well as orientation and ionic polarisation of anion A^-. Conversely, dabcoHX (X = Br^-, I^-) with spherical anions shows a different polarization order in contrast to dabcoHA. The dabco forms a one-dimensional chain, but this is a short-range order formed by weak electronic polarization of the anions. As a result, dabcoHX is a relaxor ferroelectric with proton transfer.[28-30] Thus, mono-salts consisting of dabcoH$^+$ form a polarization order due to the size, polarizability and symmetry of the anion.

Solid solutions are homogeneous mixtures of two or more components to form a single solid phase, such as the relaxor ferroelectrics of $A(BB')O_3$ described above. Curie temperature, spontaneous polarization and dielectric constant in solid solution are controlled by composition. In addition, morphotropic phase boundary (MPB) appears when crystals of different symmetry are used in solid solutions. Most physical properties such as dielectric and piezoelectric constants show an anomalous behaviour at the MPB.[31-34]

Conversely, solid solutions of molecular crystals are substitutional solid solutions of isomorphic structures with the same family elements, where phase transition behaviour and molecular motility are less dependent on composition. However, there are examples of molecular crystalline solid solutions whose phase transition behaviour and molecular mobility are composition-dependent,[35–39] for example, in solid solutions partially substituted with different halogens. CM salts (CM = cyclohexylmethylammonium) undergo a phase transition at a temperature depending on composition.[40] Furthermore, Xiong demonstrated gigantic piezoelectricity with $(TMFM)_x(TMCM)_{1-x}CdCl_3$ (TMFM = trimethylfluoromethyl ammonium, TMCM = trimethylchloromethyl ammonium).[41]

Herein, we focus on the dependence on counter anions to ferroelectric behaviours of the one-dimensional hydrogen-bonded chain of dabcoH$^+$. New halide solid solutions of dabcoH$^+$ salts were prepared and the crystal structure and phase transition behaviour were investigated by temperature variable single-crystal XRD analysis and thermal measurements. Furthermore, dielectric properties of the **$Br_{0.80}I_{0.20}$** were investigated by temperature and compositional variations.

Results and discussion

Preparation and composition determination of solid solutions.

Crystallization of dabcoHX is reported to be isolated from the aqueous solution of a 1:1 mixture of dabco with acidic HX.[28] Followed by the experimental procedures for dabcoHX, acids HX1 and HX2 were mixed at ratio *x*'. (HX = HCl, HBr, HI). Good quality single crystals which are suitable for single crystal X-ray diffraction environments were isolated after slow solvent evaporation by keeping the solution atmosphere for several days. Furthermore, EDS mapping of SEM-EDS showed uniform dispersion of both halogens within the crystal (Figure S1). The solid solution of Cl and Br is hereinafter called **ClBr** and the solid solution of Br and I is hereinafter called **BrI**.

The solid solution ratio of halide ions was estimated using CHN elemental analysis. The relationship between experimental mixing ratio *x*' and calculated solid solution ratio *x* is shown in Fig. 2. For solid solution **ClBr**, no proportional relationship between was observed the mixing ratio of the solution and the composition ratio in the crystal. The concentration of Cl was around 3 % in the Br-rich solid solution. The concentration of Br was around 7 % in the Cl-rich

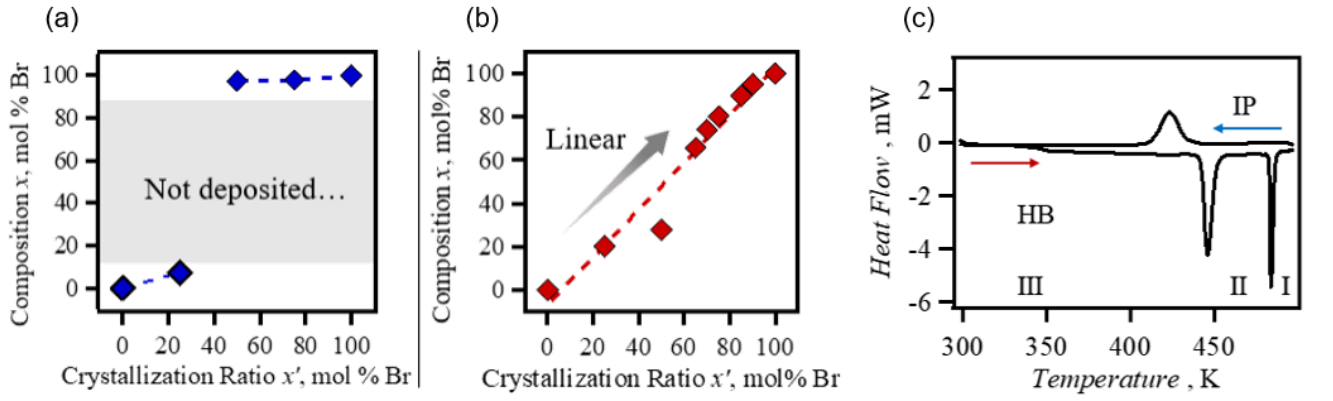

Fig. 2 (a, b) Plot of the preparation ratio (*x*') (horizontal axis) during solution preparation versus the solid solution ratio (*x*) (vertical axis) calculated by elemental analysis. (a) solid solution **ClBr**, (b) solid solution **BrI**.DSC of solid solution **ClBr**. (c) In **ClBr**, Measurements were carried out in the temperature range 273 - 500 K, at a sweep rate of 10 K/min and under N_2 atmosphere.

solid solution. These low miscibility of Cl^- and Br^- originated from differences in the structure of the end-members. In the crystal of dabcoHCl, $dabcoH^+$ interacted with Cl^-, giving an ion-pairing structure.[42] Hydrogen-bonded chain structure is observed in dabcoHCl trihydrate.[42] P-XRD showed that the diffraction pattern of the solid solution of Cl-rich corresponded to that of $(dabcoHCl)\cdot 3H_2O$. Conversely, the solid solution of Br-rich corresponded to a diffraction pattern of dabcoHBr consisting of hydrogen-bonded chains (Figure S2).

For solid solution **BrI**, a linear relationship was observed between the mixing ratio of the solution and the composition ratio in the crystal. The components are miscible in any proportion is typical for all proportional solid solutions. The high miscibility of **BrI** originated from because of its isomorphism of dabcoHBr and dabcoHI.

Crystallographic study and phase transition behaviour of ClBr.

The single crystals of the solid solution **ClBr** at Br-rich (97 % bromide) were isolated for X-ray structural analysis at 298 K. The crystal structure of the solid solution was solved with a space group *P*-6*m*2 which is the same as dabcoHBr (Figure S3). The lattice constants *a*, *c* and lattice volumes of **ClBr** were 6.6645, 5.3238 Å and 204.78 Å^3 respectively. As a result, solid solution **ClBr** was not significantly different from dabcoHBr (6.6650, 5.3130 Å and 204.40 Å^3).

The structural phase transition behaviour was investigated using DSC (Fig. 2(c)). dabcoHBr undergoes a two-step phase transition on heating at 458 K and 471 K.[28] The first transition at 458 K corresponds to the breaking of the hydrogen bond, in which $NH^+\cdots N$ hydrogen-bonded chain structure (phase-III) changed to the ion-pair structure with $NH^+\cdots Br^-$ at 458 K (phase-II). At 471 K, another hydrogen bond formed between methylene moiety and the bromide (phase-I). Furthermore, these phase transitions depend on the pressure. The lattice volume decreases by 7 Å^3 at 0.30 GPa. The transition temperature is reported to decrease by 38 K from 458 K to 420 K.[43,44] The volume change is understood with the Claussius-Clapeyron equation $dT/dP = \Delta V/\Delta S$ for the first-order phase transition. The transition from a hydrogen-bonded chain structure to an ion-pair structure is $\Delta V < 0$. Therefore, the lattice volume reduction in the hydrogen-bonded phase results in a decrease in transition temperature. In solid solution **ClBr**, corresponding two-step phase transitions were observed. The hydrogen bonding chain phase-III transited to the ion-pair phase-II at 440 K with increasing temperature. Transition enthalpy and entropy changes were estimated to ΔH = 4.6 kJ mol^{-1} and ΔS = 10.5 J mol^{-1} K^{-1}, respectively. Reported values for dabcoHBr were 458 K, 5.1 kJ mol^{-1} and 11.1 J mol^{-1} K^{-1},[28] showing corresponding ΔS. A decrease in phase transition temperature is derived from that of ΔH. Intermolecular hydrogen bonding N···N distance in **ClBr** phase III is 2.779 Å which corresponds to that in dabcoHBr. The enthalpy change by hydrogen bond is comparable. Taking the fact that $NH^+\cdots Cl^-$ is usually stronger than $NH^+\cdots Br^-$, interaction $NH^+\cdots X^-$ in **ClBr** is considered to be stronger than that of dabcoHBr. Structural details on phase-II have not been characterized due to damage to a single crystal upon phase transition.

The subsequent heating of the ion-pair phase-II leads to the next transition at 481 K in which transition enthalpy and entropy changes were 3.48 kJ mol^{-1} and 7.23 J mol^{-1} K^{-1}, respectively. These values of the dabcoHBr were reported to be 471 K, 3.33 kJ mol^{-1} and 7.07 J mol^{-1} K^{-1}. All values are increased slightly in the **ClBr**.

In the cooling process, only a single peak was observed with a phase transition temperature at 438 K with ΔH = 3.67 kJ mol^{-1}. The observed ΔH is not coincident with the some of enthalpy changes of the heating process, indicating that phase transition

Table 1 Crystallographic data for solid solution **BrI**.

Compound	$Br_{0.19}I_{0.81}$	$Br_{0.27}I_{0.73}$	$Br_{0.64}I_{0.36}$	$Br_{0.74}I_{0.26}$	$Br_{0.80}I_{0.20}$	$Br_{0.90}I_{0.10}$	$Br_{0.95}I_{0.05}$
Formula	C6H13N2Br0.19I 0.81	C6H13N2Br0.27I 0.73	C6H13N2Br0.64I 0.36	C6H13N2Br0.74I 0.26	C6H13N2Br0.80I 0.20	C6H13N2Br0.90I 0.10	C6H13N2Br0.95I 0.05
Crystal system	Hexagonal						
Space group	*P*-6*m*2						
a, Å	7.0554(4)	6.9445(9)	6.8337(5)	6.8015(6)	6.7541(6)	6.6949(4)	6.6793(6)
c, Å	5.3473(3)	5.3334(5)	5.3349(3)	5.3298(4)	5.3383(4)	5.3265(4)	5.3178(5)
V, Å^3	230.54(3)	222.75(6)	215.76(3)	213.53(4)	210.90(4)	206.76(3)	205.46(4)
Z	1						
ρ_{calc}, g cm^{-3}	1.665	1.695	1.616	1.597	1.594	1.589	1.580
Reflections collected	1334	809	1547	803	1246	778	1234
Independent reflections	245	218	240	224	231	212	225
Data/restraints/parameters	245/0/11	218/0/11	240/0/12	224/0/11	231/0/12	212/0/11	225/0/11
Goodness of fit on F_2	1.097	1.081	1.077	1.206	1.114	1.240	1.080
Final *R* indices [$I \geq 2\sigma(I)$]	R_1 = 0.0141 wR_2 = 00353	R_1 = 0.0263 wR_2 = 0.0667	R_1 = 0.0525 wR_2 = 0.1272	R_1 = 0.0436 wR_2 = 0.1136	R_1 = 0.0389 wR_2 = 0.0930	R_1 = 0.0155 wR_2 = 0.0427	R_1 = 0.0314 wR_2 = 0.0717
Final *R* indices [all data]	R_1 = 0.0141 wR_2 = 0.0353	R_1 = 0.0263 wR_2 = 0.0667	R_1 = 0.0533 wR_2 = 0.1275	R_1 = 0.0436 wR_2 = 0.1136	R_1 = 0.0394 wR_2 = 0.0933	R_1 = 0.0155 wR_2 = 0.0427	R_1 = 0.0327 wR_2 = 0.0723
Temperature, K	298						

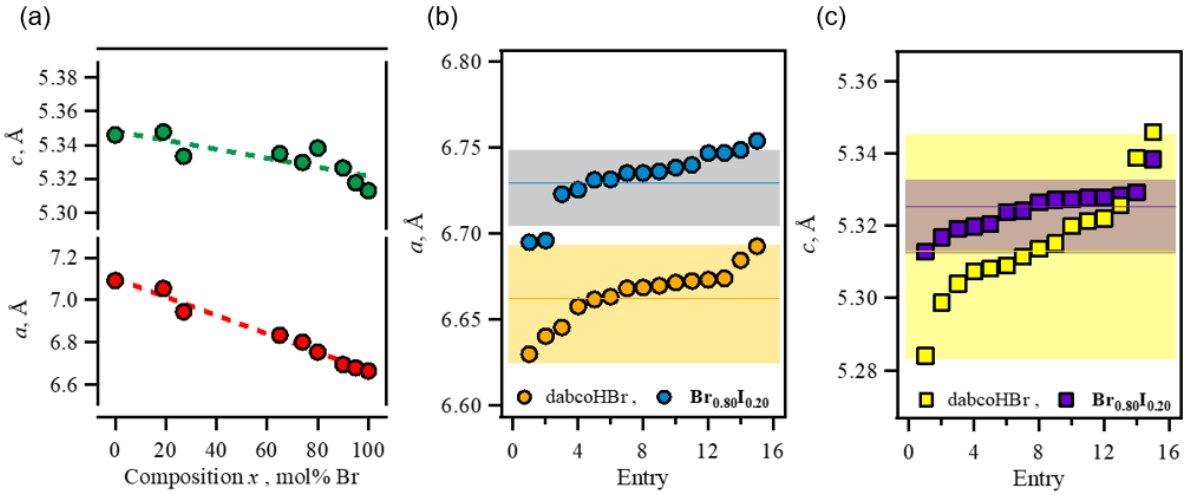

Fig. 3 (a) Composition dependence of lattice constants in solid solution **BrI**. (b, c) Dispersion of lattice constants in 15 single crystals of dabcoHBr and $\mathbf{Br_{0.80}I_{0.20}}$. The coloured range indicates a ±2σ range. Lines indicate mean values. (b) *a*-axis. (c) *c*-axis.

processes are included by the second-order type phase transition.

Crystallographic study of BrI.

The crystals obtained in solid solution **BrI** were of good quality for single crystal X-ray structure analysis in all compositions prepared. The temperature and composition dependence of the structure were evaluated at 112 - 373 K. Crystallographic data of x = 0.19, 0.27, 0.64, 0.74, 0.80, 0.90 and 0.95 at 298 K were summarised in Table 1. The crystal structure of solid solution with all compositions is isomorphic to both dabcoHBr and dabcoHI. The ratio of Br to I estimated from occupancy which is optimised by crystallographic analysis showed good agreement with the ratio obtained from elemental analysis (Table S1).

Fig. 3 (a) shows a plot of the *a*-axis length (⊥ hydrogen bonding) and *c*-axis length (// hydrogen bonding) versus composition. In dabcoHBr and dabcoHI, the difference in ionic radius of counter anions appeared remarkably to be those of *a*-axis lengths which correspond to a distance between hydrogen bonding chains. The dependence of the *a*- and *c*-axis lengths with composition was linear, which obeyed Vegard's law.

X-ray structural analysis was performed on 15 single crystals of solid solution $\mathbf{Br_{0.80}I_{0.20}}$, and also dabcoHBr, to evaluate the variation of lattice constants per crystallite. Table S2 shows the mean and standard deviation σ of the lattice constants. Fig. 3 (b, c) is a plot of the lattice lengths of dabcoHBr and $\mathbf{Br_{0.80}I_{0.20}}$ in 15 single crystals. Even for dabcoHBr, differences in lattice length were observed per single crystal. The mean, maximum/minimum and 2σ (97 %) range for the lattice lengths were 6.6649 and 5.3150, 6.6300/6.6929 and 5.2840/5.3458, 6.6323-6.6975 and 5.2846-5.3454 for the *a*- and *c*-axis respectively. This dispersion is considered to be originated from a difference in the lattice constant reflecting the measurement system and the degree of defects in single crystals. In $\mathbf{Br_{0.80}I_{0.20}}$, they were 6.7323 and 5.3246, 6.6951/6.7541 and 5.3128/5.3383, 6.7151-6.7495 and 5.3184-5.3308 on the *a*- and *c*-axis. There were also crystals where the minimum value measured with $\mathbf{Br_{0.80}I_{0.20}}$ was comparable to the maximum value measured with dabcoHBr. The dispersion of lattice constants may also derive from differences in the concentration of iodide ions. However, the fact that the standard deviation values were comparable for dabcoHBr and $\mathbf{Br_{0.80}I_{0.20}}$ suggests that differences in composition ratios per single crystal are almost negligible. The single crystal of $\mathbf{Br_{0.80}I_{0.20}}$ with the largest *a*-axis difference (entry 15) was used for the temperature dependence evaluation at 112 - 383 K (Table S3).

The temperature dependence of the lattice constant of the end-member dabcoHBr was reported by Marek Szafrański et al. [28] Both *a*- and *c*-axis lengths show a linear increase with temperature at 95-400 K (phase-III). Conversely, in $\mathbf{Br_{0.80}I_{0.20}}$, the temperature dependence of the lattice length changed at ~250 K for both the *a*- and *c*-axis (Figure S4), indicating that phase-III in dabcoHBr was divided into two

Table 2 Coefficient of thermal expansion for each lattice constant in solid solution $\mathbf{Br_{0.80}I_{0.20}}$.

	LTR	MTR
a, 10^{-5} K^{-1}	2.993	4.814
c, 10^{-5} K^{-1}	0.8285	1.822
V, 10^{-5} K^{-1}	6.864	12.40

different ranges. The low-temperature side is hereinafter called LTR (Low Temperature Range) and the temperature range at 250-383 is MTR (Medium Temperature Range). Table 2 is a summary of the coefficient of thermal expansion β calculated from the formula $\alpha = \alpha_0(1+\beta T)$. The β in dabcoHBr was constant at 4.46 × 10^{-5} K^{-1} for the *a*-axis and 1.78 × 10^{-5} K^{-1} for the *c*-axis. However, the β change from LTR to MTR in $\mathbf{Br_{0.80}I_{0.20}}$ increased 1.6- and 2.2-times on the *a*- and *c*-axis, respectively. The temperature dependence of the lattice volume V shows that corresponds to lattice lengths.

To gain details on hydrogen bond, the temperature dependence of the N···N distance between dabco molecules was investigated (Figure. S5). The N···N distance in dabcoHBr is increased linearly with

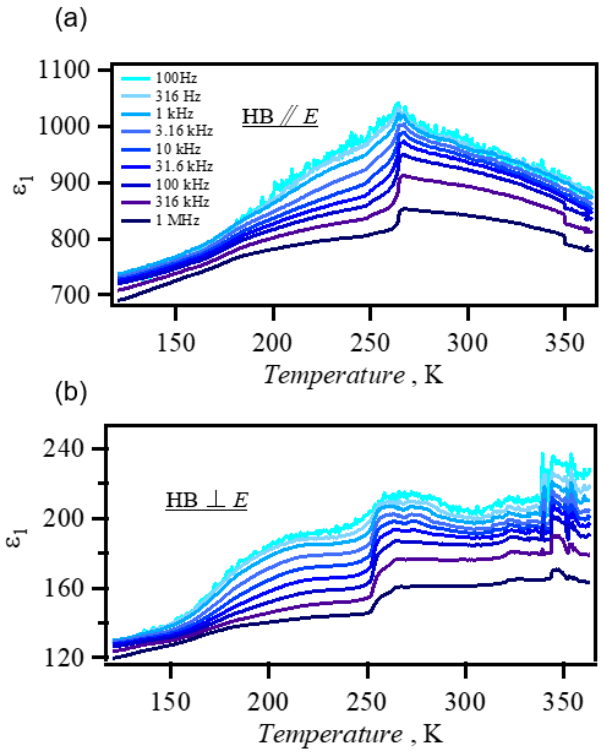

Fig. 4 (a, b) Temperature dependence of complex permittivity (a: *c*-axis direction, b: *a*-axis direction).

temperature, reaching 2.804 Å at 382 K. In **$Br_{0.80}I_{0.20}$**, the N···N distance was constant at 2.78(2) Å in LTR, increased above 250 K and was again constant at 2.81(2) Å in MTR. Elongation of the N···N distance (hydrogen bonding distance) is shown to result in weaker hydrogen bonding in MTR than in LTR. Furthermore, the elongation of the N···N distance affects the proton motility in hydrogen bonds. Activation barriers for proton motion at LTR and MTR were estimated to 0.30 and 0.37 eV by DFT (Figure S6), but there is no thermal anomaly in the DSC chart.

Dielectric properties of solid solution $Br_{0.80}I_{0.20}$.

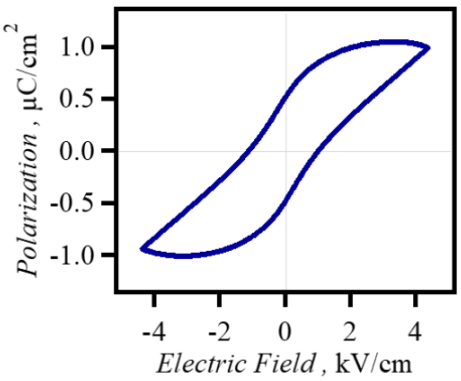

Fig. 5 *P-E* hysteresis loop of **$Br_{0.80}I_{0.20}$** measured at 298 K on the *c*-axis (20 Hz).

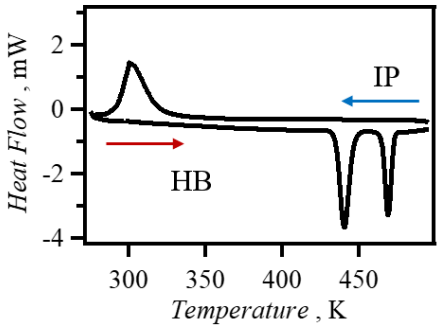

Fig. 6 In **$Br_{0.80}I_{0.20}$**, Measurements were carried out in the temperature range 273 - 500 K, at a sweep rate of 10 K/min and under N_2 atmosphere.

The end-member dabcoHBr shows a frequency-temperature dependent relaxor-like dielectric anomaly in the c-axis direction at 180 - 300 K.[28] In solid solution **$Br_{0.80}I_{0.20}$**, the temperature dependence of the complex permittivity (120 - 370 K) was evaluated using single crystals along *a*- and *c*-axis directions (Fig. 4). The **$Br_{0.80}I_{0.20}$** showed temperature- and frequency-independent dielectric anomalies in both the *a*- and *c*-axis at ~250 K. This temperature is in good agreement with that changed from LTR to MTR. In addition, a decrease of the dielectric constant was observed along the *c*-axis direction above ~250 K. This agrees with the fact in which the activation energy of proton in N···N hydrogen bond increases. *P-E* hysteresis measurements were performed in the *c*-axis direction at 298 K using single crystals (Fig. 5) The hysteresis loops were observed, indicating the ferroelectricity of MTR appeared by mixing I^-.

Phase transition behaviour of solid solution $Br_{0.80}I_{0.20}$.

Finally, the phase transition behaviours of **$Br_{0.80}I_{0.20}$** at a high temperature range above 420 K were investigated by DSC (Fig. 6). In the DSC chart, endothermal peaks were observed at 435 K and 464 K (ΔH = 5.36 and 3.18 kJ mol^{-1}, ΔS = 12.32 and 6.853 J mol^{-1} K^{-1}). P-XRD patterns measured at 480 K (Figure S7) well agree with that of phase-I of dabcoHBr, suggesting that **$Br_{0.80}I_{0.20}$** also undergoes phase transitions from hydrogen bonding structure (phase-III) to ion-paring structure of phase-I *via* phase-II. Phase transition temperatures observed for **$Br_{0.80}I_{0.20}$** were decreased by 23 and 7 K compared to those of dabcoHBr, while both of ΔH and ΔS corresponded to those of dabcoHBr.

It was reported that the phase transition temperature of dabcoHBr decreased upon lattice contraction by pressure. [44] This is due to phase-II is denser compared to phase-I. Conversely, phase transition temperature decreased even though lattice volume was increased in **$Br_{0.80}I_{0.20}$** by mixing I^-. This opposite direction from expectation is believed to be local structural distortion around I^- in **$Br_{0.80}I_{0.20}$**.

Conclusion

In summary, two solid solutions **ClBr** and **BrI** were prepared by mixing Cl^- and I^- with dabcoHBr, which has a one-dimensional

hydrogen-bonded chain structure. The composition and temperature dependence of the structure, phase transition behaviour and dielectric properties were investigated. Changes in phase transition temperatures against composition are revealed. The solid solutions **ClBr** and **BrI** showed different miscibility due to differences in the structure of the end-members. In solid solution ClBr, the miscibility in the crystals was low for all mixing ratios prepared. Mixing 3 % Cl^- with dabcoHBr resulted in an 18 K lower temperature shift in the transition temperature from the hydrogen-bonded chain structure to the ion-pair structure. However, no significant differences in structure, such as lattice constants and hydrogen bond lengths, were found. Conversely, in solid solution BrI, a linear relationship between the stocking ratio and the solid solution ratio is observed and is adjusted at any ratio. The solid solutions of all compositions were isomorphous with dabcoHBr based on the results of single-crystal X-ray structural analysis. The relationship between composition ratio and lattice constant varied linearly according to Vegard's law. In solid solution **$Br_{0.80}I_{0.20}$**, the evaluation of the temperature dependence of the structure showed the emergence at 250-373 K of a new range MTR. The MTR was a range with longer hydrogen bonds and reduced proton motion compared to LTR. Dielectric anisotropy evaluation showed the temperature of dielectric anomalies matching the temperature of the LTR to MTR. In **$Br_{0.80}I_{0.20}$**, the transition temperature from hydrogen-bonded chain structure to ion-pair structure shifted to lower temperatures due to the admixture of 20 % I^-. As these results, hydrogen bonding tuning is accommodated in the modulation of phase transition temperatures and dielectric properties.

Experimental

Synthesis of solid solution ClBr and BrI.

A mixture of dabco (1,4-diazabicyclo[2.2.2]octane) (1.127 g, 10 mmol) dissolved in water (2 mL) and the corresponding acid (HCl: 0.8 mL, HBr: 1.1 mL, HI: 1.4 mL) at 1: 1 was prepared. The crystals were obtained by solvent evaporation under shaded light for several days. Commercially available dabco, HCl, HBr and HI were used without purification. Solid solution **ClBr** was crystallised by changing the preparation ratio to HCl: 1 - *x*' and HBr: *x*' for the corresponding acids, *x*' = 0, 0.25, 0.50, 0.75, 1 (yield 37.7, 35.5, 41.8, 44.6, 46.5 %). Solid solution **BrI** was crystallised in the same way as **ClBr**, with HBr: *x*', HI: 1 - *x*', and with preparation ratios of *x*' = 0, 0.25, 0.50, 0.65, 0.70, 0.75, 0.85, 0.90, 1 (yield 42.6, 45.8, 35.2, 32.2, 31.4, 43.8, 37.5, 41.5, 46.5 %).

Measurement.

・**XRD**. Single-crystal X-ray structure analysis was performed using Rigaku XtaLAB Synergy R, DW system, Hypix, with source: Mo Kα and processing software CrysAlisPro. Powder XRD at room temperature was performed using a Rigaku Mini Flex 600 and variable temperature powder XRD was performed using a Rigaku Smart Lab, source: Cu Kα, under N_2 atmosphere.

・**SEM-EDS**. Measurements were made using a JEOL JSM-7600F and an energy-dispersive X-ray generator. Measurements were made after carbon tape was stretched over brass, a sample was placed on the tape and gold was deposited using a vacuum evaporation system (Au, Sanyu).

・**DSC**. Rigaku Thermo plus REVO2 Differential Scanning Calorimeter Measurements were carried out in an N_2 atmosphere at a sweep rate of 10 K/min using a DSCvesta instrument.

・**Complex permittivity**. Measurements were made in the frequency range of 100-1 MHz using the E4980AL Precision LCR Meter (KEYSIGHT) instrument. Measurements were performed under vacuum and temperature was controlled using a LakeShore 335 Temperature Controller.

・***P-E* Hysteresis**. Measurements were carried out using a RADIANT Precision LC II instrument.

・**DFT**. Potential energy differences (*ΔE*) were calculated by a function of B3LYP/6-31G(d,p) using N···N distances obtained from the structural analysis. The software used was Gaussian.

Conflicts of interest

There are no conflicts to declare.

Acknowledgements

The authors acknowledge the financial support from the Opto-Energy Research Centre of Yamaguchi University, JSPS KAKENHI (22H02054), the cooperative research program of the Network Joint Research Centre for Materials and Devices of Japan, and the JSPS Core-to-Core Project (International Network on Polyoxometalate Science for Advanced Functional Energy Materials).

Notes and references

1 M. Acosta, N. Novak, V. Rojas, S. Patel, R. Vaish, J. Koruza, G. A. Rossetti, Jr., and J. Rodel, *Appl. Phys. Rev.*, 2017, **4**, 041305.
2 Xian-Kui Wei, Neus Domingo, Young Sun, Nina Balke, Rafal E. Dunin-Borkowski, and Joachim Mayer, *Adv. Energy Mater.*, 2022, **12**, 2201199.
3 JAMES F. SCOTT AND CARLOS A. PAZ DE ARAUJO, *Science*, 1989, **246**, 4936.
4 Andrei Kholkin, Anna Morozovska, Dmitry Kiselev, Igor Bdikin, Brian Rodriguez, Pingping Wu, Alexei Bokov, Zuo-Guang Ye, Brahim Dkhil, Long-Qing Chen, Marija Kosec, and Sergei V. Kalinin, *Adv. Funct. Mater.*, 2011, **21**, 1977-1987.
5 Fei Li, Shujun Zhang, Dragan Damjanovic, Long-Qing Chen, and Thomas R. Shrout, *Adv. Funct. Mater.*, 2018, **28**, 1801504.
6 Hangfeng Zhang, Bin Yang, A. Dominic Fortes, Haixue Yan and Isaac Abrahams, *J. Mater. Chem. A*, 2020, **8**, 23965.
7 Hao Pan, Shun Lan, Shiqi Xu, Qinghua Zhang, Hongbao Yao, Yiqian Liu, Fanqi Meng, Er-Jia Guo, Lin Gu, Di Yi, Xiao Renshaw Wang, Houbing Huang, Judith L. MacManus-Driscoll, Long-Qing Chen, Kui-Juan Jin, Ce-Wen Nan, Yuan-Hua Lin, *Science*, 2021, **374**, 100-104.
8 Simin Wang, Fei Yan, Jin Qian, Guanglong Ge, Zhengqian Fu, Zhongbin Pan, Faqiang Zhang, Jinfeng Lin, Kun Zeng, Chukai Chen, Bo Shen, Zhifu Liu, Jiwei Zhai, *Energy Storage Materials*, 2024, **66**, 103155.
9 I-WE1 CHEN, PING LI and YING WANG, *J. Phys. Chem. Solids*, 1996, **57**(10), 1525-1536.
10 Darren J. Goossens, *Acc. Chem. Res.*, 2013, **46**(11), 2597-2606.
11 Z.-G. Ye, Y. Bing, J. Gao, and A. A. Bokov, *Phys. Rev. B*, 2003, **67**, 104104.

12 Hengxin Tan, Hiroyuki Takenaka, Changsong Xu, Wenhui Duan, Ilya Grinberg, and Andrew M. Rappe, *Phys. Rev. B*, 2018, **97**, 174101.
13 Huiyu Liu, Yangzhi Ye, Xiangyu Zhang, Tieying Yang, Wen Wen and Shan Jiang, *J. Mater. Chem. C*, 2022, **10**, 13676.
14 Xiang-Bin Han, Chao-Yang Chai, Bei-Dou Liang, Chang-Chun Fan and Wen Zhang, *CrystEngComm*, 2022, **24**, 1507.
15 Yun-Fang Zhang, Fang-Fang Di, Peng-Fei Li, and Ren-Gen Xiong, *Chem. Eur. J.*, 2021, **28**, e202102990.
16 Heng-Yun Ye, Yuan-Yuan Tang, Peng-Fei Li, Wei-Qiang Liao, Ji-Xing Gao, Xiu-Ni Hua, Hu Cai, Ping-Ping Shi, Yu-Meng You, Ren-Gen Xiong, *Science*, 2018, **361**, 151-155.
17 Hagino Morita, Ryo Tsunashima, Sadafumi Nishihara, Katsuya Inoue, Yuriko Omura, Yasutaka Suzuki, Jun Kawamata, Norihisa Hoshino, and Tomoyuki Akutagawa, *Angew. Chem. Int. Ed.*, 2019, **58**, 9184-9187.
18 Yongfa Xie, Yong Ai, Yu-Ling Zeng, Wen-Hui He, Xue-Qin Huang, Da-Wei Fu, Ji-Xing Gao, Xiao-Gang Chen, and Yuan-Yuan Tang, *J. Am. Chem. Soc.*, 2020, **142**, 12486-12492.
19 Sachio Horiuchi, Yusuke Tokunaga, Gianluca Giovannetti, Silvia Picozzi, Hirotake Itoh, Ryo Shimano, Reiji Kumai & Yoshinori Tokura, *Nature*, 2010, **463**, 789-792.
20 Sachio Horiuchi and Shoji Ishibashi, *Chem. Sci.*, 2021, **12**, 14198.
21 Sachio Horiuchi, Fumitaka Kagawa, Kensuke Hatahara, Kensuke Kobayashi, Reiji Kumai, Youichi Murakami & Yoshinori Tokura, *Nat. Commun.*, 2012, **3**, 1308.
22 Heng-Yun Ye, Yi Zhang, Shin-ichiro Noro, Kazuya Kubo, Masashi Yoshitake, Zun-Qi Liu, Hong-Ling Cai, Da-Wei Fu, Hirofumi Yoshikawa, Kunio Awaga, Ren-Gen Xiong & Takayoshi Nakamura, *Sci. Rep.*, 2013, **3**, 2249.
23 Nan Zhang, Yao Zhang, Huan-Huan Jiang, Guo-Wei Du, Qiang Pan, Ren-Gen Xiong, and Han-Yue Zhang, *Chem. Mater.*, 2022, **34**, 8077-8086.
24 Xian-Jiang Song, Zhi-Xu Zhang, Xiao-Gang Chen, Han-Yue Zhang, Qiang Pan, Jie Yao, Yu-Meng You, and Ren-Gen Xiong, *J. Am. Chem. Soc.*, 2020, **142**, 9000-9006.
25 Andrzej Katrusiak, and Marek Szafranski, *Phys. Rev. Lett.*, 1999, **82**, 576.
26 A. Katrusiak, *Journal of Molecular Structure*, 2000, **552**, 159-164.
27 Marek Szafranski, Andrzej Katrusiak, and Garry J. McIntyre, *Phys. Rev. Lett.*, 2002, **89**, 215507.
28 Marek Szafranski, *J. Phys. Chem. B*, 2009, **113**, 9479-9488.
29 Marek Szafranski, and Andrzej Katrusiak, *J. Phys. Chem. B*, 2008, **112**, 6779-6785.
30 Marek Szafranski, *Cryst. Growth Des.*, 2010, **10**(10), 4334-4338.
31 Zenghui Liu, Yi Yuan, Zeng Luo, Hongyan Wan, Pan Gao, Hua Wu, Jian Zhuang, Jie Zhang, Nan Zhang, Hongzhong Liu, Wei Ren and Zuo-Guang Ye, *J. Mater. Chem. C*, 2020, **8**, 5795.
32 Elena Aksel and Jacob L. Jones, *Sensors*, 2010, **10**, 1935-1954.
33 Le Zhang, Haoyu Wang, Dong Wang, Mengyao Guo, Xiaojie Lou, and Danyang Wang, *Adv. Funct. Mater.*, 2020, **30**, 2004641.
34 Yang Liu, Haibibu Aziguli, Bing Zhang, Wenhan Xu, Wenchang Lu, J. Bernholc & Qing Wang, *Nature*, 2018, **562**, 96-100.
35 Matteo Lusi, *Cryst. Growth Des.* 2018, **18**, 3704-3712.
36 Ryo Tsunashima, *CrystEngComm*, 2022, **24**, 1309.
37 Sa Chen, Ran Shang, Bing-Wu Wang, Zhe-Ming Wang, and Song Gao, *Angew. Chem. Int. Ed.* 2015, **54**, 11093-11096.
38 Panpan Zhao, Lulu Zhang, Zhengong Meng, and Yilong Lei, *Adv. Funct. Mater.*, 2022, **32**, 2205092.
39 Lei He, Ping-Ping Shi, Meng-Meng Zhao, Cai-Ming Liu, Wen Zhang, and Qiong Ye, *Chem. Mater.*, 2021, **33**, 799-805.
40 Haojie Xu, Wuqian Guo, Yu Ma, Yi Liu, Xinxin Hu, Lina Hua, Shiguo Han, Xitao Liu, Junhua Luo & Zhihua Sun, *Nat. Commun.*, 2022, **13**, 5329.
41 Wei-Qiang Liao, Dewei Zhao, Yuan-Yuan Tang, Yi Zhang, Peng-Fei Li, Ping-Ping Shi, Xiao-Gang Chen, Yu-Meng You, Ren-Gen Xiong, *Science*, 2019, **363**, 1206-1210.
42 Marek Szafranski, *J. Mater. Chem. C*, 2013, **1**, 7904.
43 Armand Budzianowski and Andrzej Katrusiak, *J. Phys. Chem. B*, 2006, **110**(20), 9755-9758.
44 Waldemar Nowicki, Anna Olejniczak, Michał Andrzejewski and Andrzej Katrusiak, *CrystEngComm*, 2012, **14**, 6428-6434.